Real-Time Human Foot Motion Localization Algorithm With Dynamic Speed

Luan Van Nguyen and Hung Manh La, *IEEE Senior Member*

***Abstract*—Human foot motion localization based on Inertial Measurement Unit (IMU) sensor especially in large environments is a challenging and interesting research topic. In this paper, we propose a human foot motion localization algorithm to accurately estimate the human foot position, velocity and attitude in a real-time manner. The proposed algorithm integrates Inertial Navigation System (INS), Gait Phase Detection (GPD), Zero Velocity Update (ZVU) and Extended Kalman filter (EKF) to deal with IMU drift problems as well as noise from indoor and outdoor environments with local magnetic disturbances. The proposed algorithm is validated with the Motion Tracking System (Ground Truth). Experimental results are conducted in both indoor and outdoor environments to further demonstrate the localization performance of our proposed algorithm. Our algorithm can be embedded in wearable sensor devices for other practical applications.**

Keywords: **Real-time localization, Human foot motion localization, EKF, Zero velocity update, Inertial navigation system, Gait phase detection.**

I. Introduction

A. Motivation

The tracking of human foot motion trajectory is known as a Pedestrian Dead-Reckoning problem [1]. The solution for this problem integrates the step length, velocity and orientation of the human foot to estimate position of human motion by time. There are different technologies (e.g. ultrasound, radio or vision technology) for this solution. Especially since the Micro Electro Mechanical System (MEMS) technology has been born, the human foot motion tracking based on the Inertial/Magnetic Measurement Units (IMMUs) sensors has been researched and has some significantly published results [2]–[5]. The IMMUs technology is independent to the pre-installed infrastructure and convenient for wearable sensor devices. It has been applied for applications of localization and navigation of human motion [6]–[8].

Reaching high accuracy of human foot motion localization based on the IMU sensors especially in the environments with local magnetic disturbances is a challenging research topic. There are some existing work [3]–[5] researched on and proposed the solutions to increase the accuracy of human foot motion localization based on the IMU sensors. The accuracy of human foot motion trajectory using IMU is variety, and its error is usually greater than 10% of total travel length. Besides, the localization algorithm for mobile devices and wearable sensor on human motion is proposed [9], [10]. In summary, the existing algorithms have some disadvantages as they are usually off-line algorithms which are designed to work only on off-line data set. Additionally, they only work with a certain foot motion speed. Hence, our focus in this paper is to develop a human foot motion localization algorithm which can achieve higher accuracy and real-time data processing with dynamic human motion speed for practical applications.

The main contribution of this paper is the development of real-time algorithm for accurate human foot motion localization in disturbed environments. Additionally, the proposed algorithm works with different speeds of motion and can process real-time stream data from IMU device. Our proposed approach relies on dynamic human Gait Phase Detection (GPD), Zero Velocity Update (ZVU) and Extended Kalman Filter (EKF). GPD allows to detect human gait motion (stance and swing phases) by measuring actual position and attitude of foot motion, and then ZVU helps remove the accumulative error from IMU over time. The integrated EKF is to deal with IMU drift and noise of environments.

B. Literature Review

Indoor localization has many potential applications such as search and rescue in fire or in emergency, navigation for visitor, security purpose, and mobile 3D radio tour guide, etc. There are variety of literature and techniques proposed for the indoor localization. These techniques may apply a very simple, light and wearable sensor or a very complicated system. There may be a radio system, ultrasonic radio systems, Bluetooth systems, Wireless and RFID systems. These systems [11]–[15] have high accuracy but they require a high cost of deploy and a complicated maintenance. These expenditures prohibit their potential applications in indoor environments.

Another method for indoor localization is tracking system which based on the Pedestrian Dead-Reckoning (PDR) technique. The localization systems based on PDR are simple and don't require to setup any complicated infrastructure. They have just combined the knowledge of walking gait phase of PDR with a light and wearable inertial sensor such as an IMU mounted on a foot. Then they integrate the position of foot from receiving data of this sensor by INS technique. These systems usually apply a gait phase detection technique, and Zero Velocity Update (ZVU) for their integrations. However, the accuracy of INS and ZVU methods [1]–[5], [16]–[33] is not high enough. A reason is the drift of IMU devices. The errors of IMU drift are accumulated by time. The other techniques applying Bayesian Filters such an Extended

L. Nguyen and H. La are with with the Department of Computer Science and Engineering, University of Nevada, Reno, NV 89557, USA. Corresponding author: Hung La, email: hla@unr.edu.

Kalman Filter [3], [5], [11], [24], [30], [38], [39], Unscented Kalman Filter [40], or Particle Filters [41] reduce the errors from IMU drift.

There are some literature proposed an integration of both GPS and IMU for navigation of human motion [33]–[35]. They can be applied for localization in outdoor environments. However, the GPS does not help for indoor localization. Some other literature [36], [37] proposed the simultaneous localization and mapping (SLAM) principle using laser scanners to increase the accuracy of localization. But these methods require to attach more devices on human foot such as a camera or a laser scanner. They are not convenient for wearing person and its data is usually large that makes it very difficult for real-time processing.

The remaining of the paper is organized as follows. The next section presents an overview of the human foot motion localization scheme. Section III presents human gait motion analysis. Section IV presents the real-time human foot motion localization algorithm. Section V applies the Motion Tracking System to verify our algorithm's accuracy. Section VI presents experimental results to demonstrate the effectiveness of the proposed algorithm, and the comparison with other existing algorithms is given. Finally, the conclusion is given in Section VII.

II. Overview of Human Foot Motion Localization Scheme using IMU

The overview of the human foot foot motion localization scheme is shown in Fig. 1. The localization scheme has four modules as follows. The first module is IMU device including three embedded sensors: Accelerometers measuring the acceleration $\boldsymbol{a}_b^t$, Gyroscopes measuring the angular rate $\boldsymbol{w}_b^t$, and Magnetometer measuring the magnetic of the Earth $\boldsymbol{m}_b^t$.

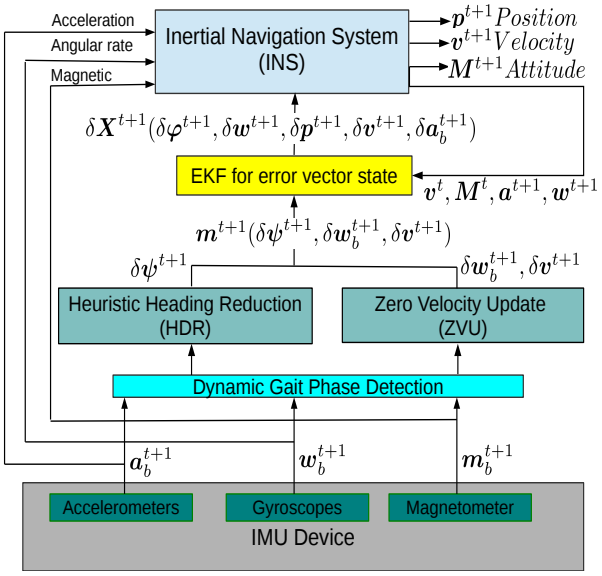

Fig. 1. The INS/EKF ZVU HDR algorithm

The super index b here is referenced to a value coordinate system in the body frame of IMU device. The super index t is the value at a discrete times t in the IMU measurement time life. Some IMU models available on the market are also integrated the Global Position System (GPS) and other additional sensors. However, in this paper we mainly consider on the algorithm working environments where GPS sensor is not available.

The second module includes a dynamic Gait Phase Detection (GPD), a Zero Velocity Update (ZVU), and a Heuristic Heading Reduction (HDR). GPD receives measurements $\boldsymbol{a}_b^t$, $\boldsymbol{w}_b^t$, and $\boldsymbol{m}_b^t$ from IMU devices to detect the stance and still phase of human gait. Then, ZVU and HDR utilize the human gait motion detection to estimate the error measurement vectors.

The third module is Extended Kalman Filter (EKF) which is designed to estimate the errors of actual acceleration, velocity and position of human foot motion by taking feedback from Inertial Navigation System (INS). The last module is an INS which receives IMU data (including the acceleration $\boldsymbol{a}_b^t$, angular rate $\boldsymbol{w}_b^t$ and earth magnetic $\boldsymbol{m}_b^t$) and the state measurement errors from the EKF to output the final estimations of velocity, attitude, and position of human foot motion.

III. Human Gait Motion Analysis

A. Inertial Navigation System (INS)

Generally, the INS system accepts the data from three sensors Accelerometers, Gyroscope, and Magnetometer inside the IMU as the input data. This input data usually includes acceleration $\boldsymbol{a}_b^{t+1}$, angular rate $\boldsymbol{w}_b^{t+1}$, magnetic field $\boldsymbol{m}_b^{t+1}$, and the quaternion $\boldsymbol{q}^{t+1}$. The super index $^{t+1}$ is a discrete responding time of IMU at $t+1$. The super index $_b$ represents this data in body frame coordinate system of IMU. The quaternion is a vector $\boldsymbol{q}^{t+1}(x, y, z, w)$. The conjugation $(\boldsymbol{q}^{t+1})^*$ of $\boldsymbol{q}^{t+1}$ is a quaternion and it can be obtained:

$$(\boldsymbol{q}^{t+1})^* = (-\boldsymbol{q}^{t+1}(x), -\boldsymbol{q}^{t+1}(y), -\boldsymbol{q}^{t+1}(z), \boldsymbol{q}^{t+1}(w)). \quad (1)$$

The Euler angles of rotation, $Roll$ (α^{t+1}), $Pitch$ (β^{t+1}) and Yaw (γ^{t+1}) rotate along the X, Y, Z axis, respectively. They can be obtained by:

$$\begin{bmatrix} \alpha^{t+1} \\ \beta^{t+1} \\ \gamma^{t+1} \end{bmatrix} = \begin{bmatrix} f_1(\boldsymbol{q}^{t+1}(x)) \\ f_2(\boldsymbol{q}^{t+1}(x)) \\ f_3(\boldsymbol{q}^{t+1}(x)) \end{bmatrix} \quad (2)$$

where, $f_1(\boldsymbol{q}^{t+1}) = atan2[2(\boldsymbol{q}^{t+1}(x)\boldsymbol{q}^{t+1}(y) + \boldsymbol{q}^{t+1}(z)\boldsymbol{q}^{t+1}(w)), 1 - 2((\boldsymbol{q}^{t+1}(y))^2 + (\boldsymbol{q}^{t+1}(z))^2)]$,
$f_2(\boldsymbol{q}^{t+1}) = arcsin[2(\boldsymbol{q}^{t+1}(x)\boldsymbol{q}^{t+1}(z) - \boldsymbol{q}^{t+1}(w)\boldsymbol{q}^{t+1}(y)]$,
$f_3(\boldsymbol{q}^{t+1}) = atan2[2(\boldsymbol{q}^{t+1}(x)\boldsymbol{q}^{t+1}(z) + \boldsymbol{q}^{t+1}(y)\boldsymbol{q}^{t+1}(z)), 1 - 2((\boldsymbol{q}^{t+1}(z))^2 + (\boldsymbol{q}^{t+1}(w))^2)]$.

The velocity of motion in body frame can be computed:

$$\boldsymbol{v}_b^{t+1} = \int \boldsymbol{a}_b^{t+1} dt. \quad (3)$$

The transformation of acceleration $\boldsymbol{a}_b^{t+1}$ from the IMU body frame into the North East Down (NED) coordinate frame system [4], [42] can be obtained:

$$\boldsymbol{a}_e^{t+1} = \boldsymbol{q}^{t+1}.\boldsymbol{a}_b^{t+1}.(\boldsymbol{q}^{t+1})^*. \quad (4)$$

From (4), the real motion acceleration in earth coordinate system NED can be obtained as

$$\boldsymbol{a}_m^{t+1} = \boldsymbol{a}_e^{t+1} - \boldsymbol{g}_e, \quad (5)$$

where, $\boldsymbol{g}_e$ is the gravitational acceleration:

$$\boldsymbol{g}_e = (0.0, 0.0, 9.8m/s^2). \quad (6)$$

The velocity of human motion can be obtained as:

$$\boldsymbol{v}_m^{t+1} = \int \boldsymbol{a}_m^{t+1} dt. \quad (7)$$

The position of foot motion in real time can be obtained as:

$$\boldsymbol{p}^{t+1} = \int \boldsymbol{v}_m^{t+1} dt. \quad (8)$$

This $\boldsymbol{p}^{t+1}$ is a 3D vector position of foot in the NED coordinate system.

B. Dynamic Gait Phase Detection (DGP)

Due to the drift of real-time IMU data of acceleration, angular rate and magnetic field, we can not rely on only the INS to estimate the position of human foot. Besides, the IMU data is also effected by the position, attitude on the Earth and the objects in surrounding environments such as steel frame inside building and moving objects, etc. It is worth to note that human gait is composed by two phases, stance and swing phases [43] as show in Fig. 2. In the stance phase, human foot stands on the ground and doesn't move. This means that the actual velocity of human foot in this phase must be zero. Hence, if the velocity of the foot is detected larger than zero in this phase, it must be the error velocity coming from IMU drift.

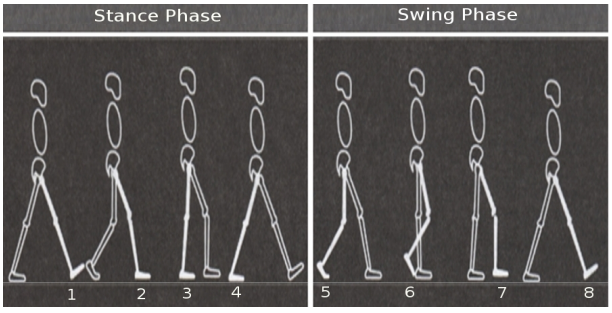

Fig. 2. The Human Motion Gait Phase

The human gait is depending on the human motion speed. There is a very important question of how to detect the stance phase of each human gait in different motion speed. In [4] the stance phase detection algorithm is limited to normal walking speed motion, and it may not work for fast changing speeds. In [3] a method using both acceleration and angular rate to check for stance phase of human gait is proposed. This method requires some pre-determined thresholds for checking the magnitude of acceleration, local acceleration, and gyroscope. Obviously, it will meet problem with different people, and different speed of motion. In this paper, we propose an efficient method to detect gait phases of human foot motion in which the threshold values are automatically computed and updated by real-time operation and human motion speed. Therefore, our proposed algorithm can work with any human motion like walking or running.

We first presents the dynamic change of sensor data which includes changes of local acceleration ($|\boldsymbol{a}_{local}^{t+1} - \boldsymbol{a}_{local}^{t}|$), of magnitude of acceleration ($|\boldsymbol{a}_m^{t+1} - \boldsymbol{a}_m^t|$), and of angular rate magnitude ($|\boldsymbol{w}_m^{t+1} - \boldsymbol{w}_m^t|$). Then the dynamic gain d_g^{t+1} at time $t+1$ can be defined as

$$d_g^{t+1} = |\boldsymbol{a}_{local}^{t+1} - \boldsymbol{a}_{local}^{t}| + |\boldsymbol{a}_m^{t+1} - \boldsymbol{a}_m^t| + |\boldsymbol{w}_m^{t+1} - \boldsymbol{w}_m^t|. \quad (9)$$

The local acceleration $\boldsymbol{a}_{local}^{t+1}$ is computed:

$$(\boldsymbol{a}_{local}^{t+1})^2 = \frac{1}{2s+1} \sum_{j=t-2s}^{t+1} (\boldsymbol{a}_b^{t+1} - \boldsymbol{a}_{eva}^{j})^2. \quad (10)$$

Note that Equ. (10) is computed in real-time and just requires data for computing local acceleration from some previous time steps. This is a main difference comparing to the off-line algorithms in [4] [3], [5]. Superindex j in Equ. (10) above is from time $t+1$ dating back to $(2s+1)$ previous time steps.

The $\boldsymbol{a}_{eva}^{j}$ in Equ. (10) is computed by:

$$\boldsymbol{a}_{eva}^{j} = \frac{1}{2s+1} \sum_{k=j-2s-1}^{j} \boldsymbol{a}_b^k. \quad (11)$$

Then the dynamic gain d_g^{t+1} at times t is used to compute the values of stance condition s_c^{t+1} from the five nearest previous values of d_g^{t+1}:

$$s_c^{t+1} = \frac{d_g^{t+1} + ... + d_g^{t-3}}{5}. \quad (12)$$

We assume that time $t+1$ is a discrete time during step i of motion. The dynamic threshold of stance condition s_c^{t+1} at time $t+1$ in step i is the average value of all s_c^t in step $i-1$ and threshold th^{i-1}:

$$th^i = \frac{th^{i-1} + s_a^{i-1}}{2}, \quad (13)$$

where, the initial value of th^0 can be setup by 0.8 or by th^i of previous working time of algorithm and s_a^{i-1} is the average of the stance condition in previous step $i-1$. It can be obtained by formula:

$$s_a^{i-1} = \frac{\sum_{t^{i-1}=1}^{k} s_c^{t^{i-1}}}{k}, \quad (14)$$

where, $s_c^{t^{i-1}}$ is stance condition at a discrete time of previous step $i-1$. We assume there are k discrete times at step $i-1$.

The threshold th^i is computed and updated at the end of stance phase of previous step $i-1$. Since th^i is dynamic threshold, it helps the foot motion localization algorithm (discussed in Section IV) adapt to speed changes of foot motion. This threshold is free from any pre-definded threshold value and it only depends on the speed of motion. It increases when the motion speed increases and otherwise. So it can work with any people gait, any walking speed, and any IMU device.

The gait detection g_d^{t+1} can be obtained by:

$$g_d^{t+1} = \begin{cases} 0, & sc^{t+1} \leq th^i \text{ (stance phase)} \\ 6, & otherwise \text{ (swing phase)} \end{cases} \quad (15)$$

when $g_d^{t+1} = 0$ it is in the stance phase, and $g_d^{t+1} = 6$ it is in the swing phase.

The summary of the dynamic gate phase (DGP) detection algorithm is presented in Algorithm 1. The detection result of swing and stance phases using this DGP algorithm is shown in Fig. 3. In this figure, the result for three different speeds: (a) fast speed (1.79m/s), (b) normal speed (1.28m/s), and (c) slow speed (0,58m/s) are showed for the 3s moving duration. There are 3.2 gait circles for fast speed, 2.5 gait circles for normal speed, and only 1.8 gait circle for slow speed. One fast speed circle has a distance about 1.8 m. One normal gait circle has a distance about 1.1 m. And one slow gait circle has distance about 0.85 m. The values of dynamic threshold is changed a little bit after each gait circle.

C. Zero Velocity Update (ZVU) Algorithm

Whenever the stance phase is detected, the Zero Velocity Update (ZVU) algorithm [2], [3], [5] will measure the state errors. Here we assume that each gait of human motion has a duration $[T-\delta T, T]$, where T is a discrete time at the end of the stance phase. Then we can compute the bias error a_{be}^{t+1} of acceleration at times $t+1=T$ of foot motion in stance phase:

$$\boldsymbol{a}_{mbe}^{t+1} = \frac{\boldsymbol{v}_m^{t+1=T}}{T}. \quad (16)$$

We can compute the Earth bias error acceleration:

$$\boldsymbol{a}_{ebe}^{t+1} = \boldsymbol{a}_{mbe}^{t+1} + \boldsymbol{g}_e. \quad (17)$$

where, the $\boldsymbol{g}_e$ is in Equ. (6). The bias error acceleration in body frame from time $t+1$ for next step can be obtained:

$$\boldsymbol{a}_{bbe}^{t+1} = (\boldsymbol{q}^{t+1})^* . \boldsymbol{a}_{ebe}^{t+1} . \boldsymbol{q}^{t+1}. \quad (18)$$

The bias error velocity which is also the drifted velocity $\delta \boldsymbol{v}^{t+1}$ in body frame from time $t+1$ for next step can be on stained:

$$\delta \boldsymbol{v}_b^{t+1} = \boldsymbol{v}_{bbe}^{t+1} = \int \boldsymbol{a}_{bbe}^{t+1} dt. \quad (19)$$

The actual motion value of acceleration $\boldsymbol{a}_a^{t+1}$, velocity $\boldsymbol{v}_a^{t+1}$ and position $\boldsymbol{p}_a^{t+1}$ at each time t need to be recalculated and updated by equation:

$$\boldsymbol{a}_a^{t+1} = \boldsymbol{a}_m^{t+1} - \boldsymbol{a}_{mbe}^{t+1}. \quad (20)$$

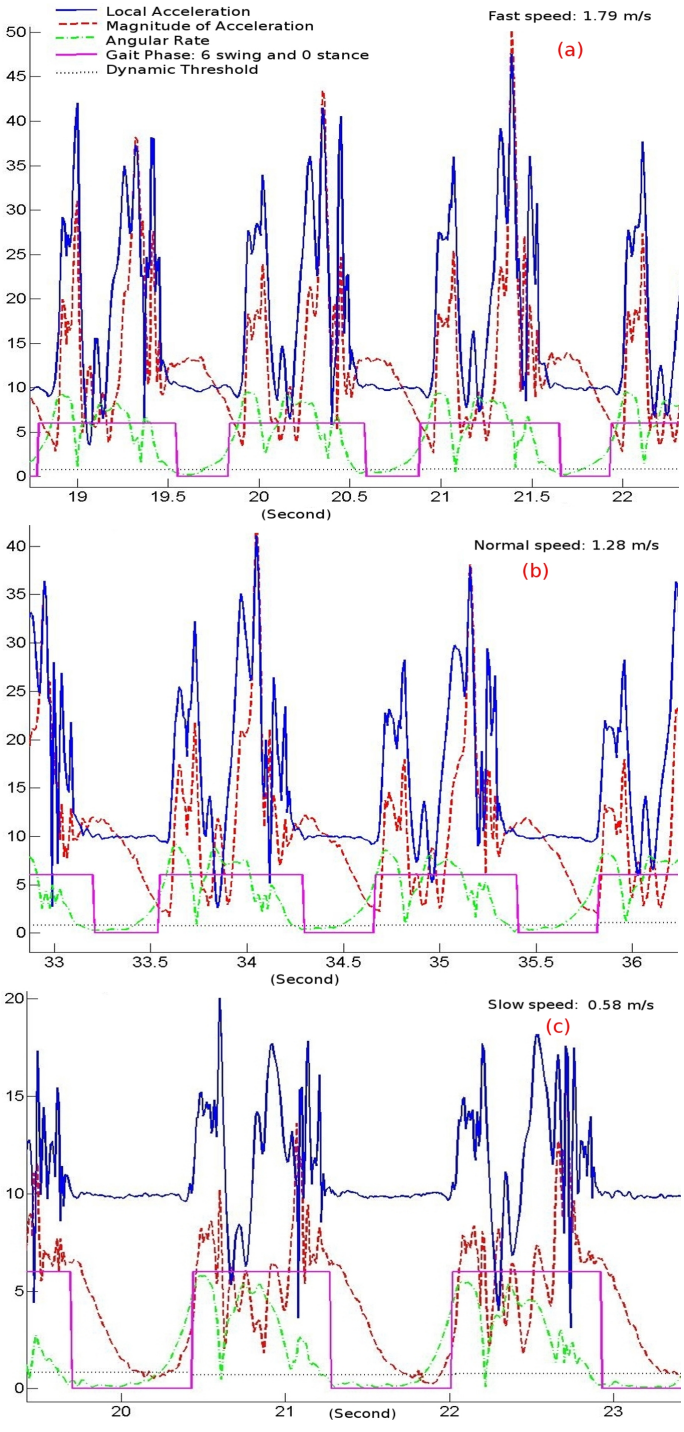

Fig. 3. The Human Motion Gait Phase Detection

Also Equ. (7, 8) for actual velocity and position will be computed by the new actual acceleration $\boldsymbol{a}_a^{t+1}$. The actual velocity of human motion can be obtained as:

$$\boldsymbol{v}_a^{t+1} = \int \boldsymbol{a}_a^{t+1} dt. \quad (21)$$

The actual position of foot motion in real time can be

Algorithm 1: DYNAMIC GAIT PHASE (DGP) DETECTION

Input: Real-time acceleration, angular rate vectors at discrete times $t+1$ in IMU body system $\langle a_b^{t+1}, w_b^{t+1}\rangle$

Output: $True$:Stance Phase, $False$:Swing Phase

if $t+1 \geq 2s+1$ **then**
  $j \leftarrow t$
  while $(j \leq t) and (j \geq (t-s))$ **do**
    $k \leftarrow (j-s)$
    while $k \leq j$ **do**
      $\boldsymbol{a}_{eva}^{j} \leftarrow \boldsymbol{a}_{eva}^{j} + \boldsymbol{a}_b^k$
      $k \leftarrow (k+1)$
    $\boldsymbol{a}_{eva}^{j} \leftarrow \frac{1}{2s+1}\boldsymbol{a}_{eva}^{j}$
    $(\boldsymbol{a}_{local}^{t+1})^2 \leftarrow (\boldsymbol{a}_{local}^{t+1})^2 + (\boldsymbol{a}_b^{t+1} - \boldsymbol{a}_{eva}^{j})^2$
    $j \leftarrow (j-1)$
  $(\boldsymbol{a}_{local}^{t+1})^2 \leftarrow \frac{1}{2s+1}(\boldsymbol{a}_{local}^{t+1})^2$
else
  $j \leftarrow t$
  $k \leftarrow 0$
  while $k \leq j$ **do**
    $\boldsymbol{a}_{eva}^{j} \leftarrow \boldsymbol{a}_{eva}^{j} + \boldsymbol{a}_b^k$
    $k \leftarrow (k+1)$
  $(\boldsymbol{a}_{local}^{t+1})^2 \leftarrow \frac{1}{k+1}\boldsymbol{a}_{eva}^{j}$
$d_g^{t+1} \leftarrow |\boldsymbol{a}_{local}^{t+1} - \boldsymbol{a}_{local}^{t}| + |\boldsymbol{a}_m^{t+1} - \boldsymbol{a}_m^{t}| + |\boldsymbol{w}_m^{t+1} - \boldsymbol{w}_m^{t}|$
$s_c^{t+1} \leftarrow \frac{d_g^{t+1} + ... + d_g^{t-3}}{5}$
$th^i \leftarrow \frac{th^{i-1} + s_a^{i-1}}{2}$
if $s_c^{t+1} \leq th^i$ **then**
  return *True*
else
  return *False*

obtained as:

$$\boldsymbol{p}^{t+1} = \int \boldsymbol{v}_a^{t+1} dt. \tag{22}$$

D. Heuristic Heading Reduction (HDR)

It is note that the characteristic of human motion is usually on the straight direction. From this characteristic the Heuristic Heading Reduction (HDR) [3], [44] is applied to help adjust Yaw (γ) angle of heading direction. If the magnetic field of surrounding environment makes change in heading direction, it will effect the bias of γ angle direction. Hence we can rely on the comparison of γ angle at the stance of time step T_i with two previous γ angles at the stance of time step $T_{(i-1)}$ and $T_{(i-2)}$. The difference of γ angles can help adjust the bias of γ angle in the next time step γ^{t+1}. Or, the HDR can be defined by

$$\delta\psi^{t+1} = \delta\psi_{\gamma^{T_i}} = \gamma^{T_i} - \frac{\gamma^{T_{(i-1)}} + \gamma^{T_{(i-2)}}}{2}. \tag{23}$$

where the T_i is the last discrete times of stance phase of step i. Based on the observation of the normal straight ahead walking, we define a threshold for straight ahead bias of γ angle as $th_\gamma = 0.5rad$. From this threshold value, we need to adjust γ angle of each discrete time $t+1$ for acceleration of the swing phase.

This also means that we need to update all acceleration, velocity, and position from Equ. (4), (5), (7), and (8) inside the swing phase of each step. We use a superindex $_{DHR}$ for adjusting all above formulas.

$$\boldsymbol{a}_{eHDR}^{t+1} = \boldsymbol{M}_{NED}^{1|0}.\boldsymbol{a}_b^{t+1}. \tag{24}$$

where, $\boldsymbol{M}_{NED}^{1|0}$ can be obtained by Equ. (40). But α, β, and γ need to be changed:

$$\alpha = \alpha^{t+1}, \beta = \beta^{t+1}, \gamma = \gamma^{t+1} + \delta\psi^{t+1} \tag{25}$$

where, α^{t+1}, β^{t+1}, and γ^{t+1} are in Equ. (2). The real motion acceleration in the Earth coordinate system NED can be obtained:

$$\boldsymbol{a}_{mHDR}^{t+1} = \boldsymbol{a}_{eHDR}^{t+1} - \boldsymbol{g}_e, \tag{26}$$

where, $\boldsymbol{g}_e$ is in Equ. (6). The velocity of human motion can be obtained as:

$$\boldsymbol{v}_{mHDR}^{t+1} = \int \boldsymbol{a}_{mHDR}^{t+1} dt. \tag{27}$$

The position of foot motion in real time can be obtained as:

$$\boldsymbol{p}_{HDR}^{t+1} = \int \boldsymbol{v}_{mHDR}^{t+1} dt. \tag{28}$$

IV. REAL-TIME HUMAN FOOT MOTION LOCALIZATION ALGORITHM WITH DYNAMIC SPEED

In this section, we present a real-time human foot motion localization algorithm applied our proposed method for dynamic gait detection. We name it as a Real-Time Dynamic INS/EKF+ZVU+HDR Algorithm. The diagram of this algorithm can be seen in Fig. 4. The ZVU applied in the dynamic stance phase detection of human gait at time $t+1$ of IMU's output frequency can estimate the drift error of velocity $\delta\boldsymbol{v}_b^{t+1}$ and angular rate $\delta\boldsymbol{w}_b^{t+1}$.

$$\delta\boldsymbol{v}_b^{t+1} = \boldsymbol{v}_b^{t+1} - \boldsymbol{v}_a^{t+1}, \tag{29}$$

where $\boldsymbol{v}_a^{t+1}$ is actual velocity of the foot in the stance phase, or $\boldsymbol{v}_a^{t+1} = [0\ 0\ 0]^T$. Similarly we have:

$$\delta\boldsymbol{w}_b^{t+1} = \boldsymbol{w}_b^{t+1} - \boldsymbol{w}_a^{t+1}, \tag{30}$$

where $\boldsymbol{w}_a^{t+1}$ is actual angular rate of the foot in the stance phase, or $\boldsymbol{w}_a^{t+1} = [0\ 0\ 0]^T$.

The HDR can be applied to compute the heading error of foot motion, in X axis or Yaw (γ) angle. The drifted errors of the yaw angle $\delta\psi^{t+1}$ obtained by HDR, and drift error

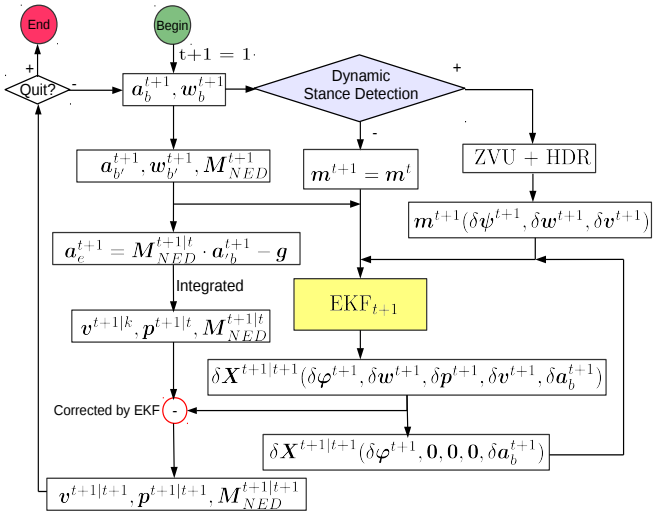

Fig. 4. The Real-Time Dynamic INS/EKF+ZVU+HDR algorithm.

of velocity $\delta \boldsymbol{v}_b^{t+1}$ and drift error of of angular rate $\delta \boldsymbol{w}_b^{t+1}$ obtained by ZVU form a vector of actual error measurement $\boldsymbol{m}^{t+1}$ for the EKF.

$$\boldsymbol{m}^{t+1} = (\delta\psi^{t+1}, \delta \boldsymbol{w}_b^{t+1}, \delta \boldsymbol{v}^{t+1}). \tag{31}$$

The output of the EKF estimation at time t is a 15 elements error state vector $\delta \boldsymbol{X}^{t|t}$. This error state vector is used to correct the estimated values of velocity, position, and attitude for the INS module (see Fig. 1).

$$\delta \boldsymbol{X}^{t|t} = \delta \boldsymbol{X}^t(\delta\boldsymbol{\varphi}^t, \delta \boldsymbol{w}^t, \delta \boldsymbol{p}^t, \delta \boldsymbol{v}^t, \delta \boldsymbol{a}_b^t). \tag{32}$$

where $\delta\boldsymbol{\varphi}^t$, $\delta \boldsymbol{w}^t$, $\delta \boldsymbol{p}^t$, $\delta \boldsymbol{v}^t$, and $\delta \boldsymbol{a}_b^t$ represent attitude, angular rate, position, velocity, and acceleration error, respectively. The error state transition of the EKF at time $(t+1)$ is obtained:

$$\delta \boldsymbol{X}^{t+1|t} = \boldsymbol{\Phi}^{t+1} \delta \boldsymbol{X}^{t|t} + \boldsymbol{w}_t. \tag{33}$$

where $\delta \boldsymbol{X}^{t+1|t}$ is the predicted error state at time $t+1$, $\delta \boldsymbol{X}^{t|t}$ is the EKF state error at time t, and $\boldsymbol{w}_t$ is the process noise with covariance matrix $\boldsymbol{Q}_t = \boldsymbol{E}(\boldsymbol{w}^t(\boldsymbol{w}^t)^T)$. The $\boldsymbol{\Phi}^{t+1}$ with its size of 15×15 defined in Equ. (34).

$$\boldsymbol{\Phi}^{t+1} = \begin{bmatrix} \boldsymbol{I} & \boldsymbol{\Phi}^{t+1}(01) & \boldsymbol{0} & \boldsymbol{0} & \boldsymbol{0} \\ \boldsymbol{0} & \boldsymbol{I} & \boldsymbol{0} & \boldsymbol{0} & \boldsymbol{0} \\ \boldsymbol{0} & \boldsymbol{0} & \boldsymbol{I} & \boldsymbol{\Phi}^{t+1}(23) & \boldsymbol{\Phi}^{t+1}(24) \\ \boldsymbol{\Phi}^{t+1}(31) & \boldsymbol{0} & \boldsymbol{0} & \boldsymbol{I} & \boldsymbol{\Phi}^{t+1}(34) \\ \boldsymbol{0} & \boldsymbol{0} & \boldsymbol{0} & \boldsymbol{0} & \boldsymbol{\Phi}^{t+1}(44) \end{bmatrix} \tag{34}$$

where, $\boldsymbol{I}$ is a 3×3 unit matrix, $\boldsymbol{0}$ is a 3×3 zero matrix.
$\boldsymbol{\Phi}^{t+1}(01) = \Delta t \cdot \boldsymbol{M}_{NED}^{t+1|t}; \boldsymbol{\Phi}^{t+1}(23) = \Delta t \cdot \boldsymbol{I}$
$\boldsymbol{\Phi}^{t+1}(24) = \dfrac{-\Delta t^2}{2} \cdot \boldsymbol{S}(a_{n'}^{t+1}); \boldsymbol{\Phi}^{t+1}(31) = -\Delta t \cdot \boldsymbol{S}(a_{n'}^{t+1})$
$\boldsymbol{\Phi}^{t+1}(34) = \Delta t \cdot \boldsymbol{M}_{NED}^{t+1|t} \boldsymbol{\Phi}^{t+1}(44) = -\Delta t \cdot \boldsymbol{S}(a_{n'}^{t+1})$.

The term $\boldsymbol{S}(a_{n'}^{t+1})$ in Equ. 34 is the skew symmetric matrix for accelerations to enable the EKF to estimate $Roll$ and $Pitch$.

$$\boldsymbol{S}(\boldsymbol{a}_{n'}^{t+1}) = \begin{bmatrix} 0 & -\boldsymbol{a}_{n'}^{t+1}(2) & \boldsymbol{a}_{n'}^{t+1}(1) \\ \boldsymbol{a}_{n'}^{t+1}(2) & 0 & -\boldsymbol{a}_{n'}^{t+1}(2) \\ -\boldsymbol{a}_{n'}^{t+1}(1) & \boldsymbol{a}_{n'}^{t+1}(0) & 0 \end{bmatrix} \tag{35}$$

where, $\boldsymbol{a}_{n'}^{t+1}$ is the bias-corrected acceleration in the navigation frame or the NED frame.

$$\boldsymbol{a}_{n'}^{t+1} = \boldsymbol{M}_{NED}^{t+1|t} \cdot \boldsymbol{a}_{b'}^{t+1} \tag{36}$$

where, $\boldsymbol{M}_{NED}^{t+1|t}$ is a transformation matrix defined in Equ. (38). At time $t+1$ of IMU output data, we get raw value of acceleration and angular rate from IMU in its body frame: $\boldsymbol{a}_b^{t+1}$, $\boldsymbol{w}_b^{t+1}$, respectively.

We then compute the bias compensation for acceleration $\boldsymbol{a}_{b'}^{t+1}$ and angular rate $\boldsymbol{w}_{b'}^{t+1}$ from the EKF error state vector $\delta \boldsymbol{X}^{t|t}$ in Equ. (32):

$$\boldsymbol{w}_{b'}^{t+1} = \boldsymbol{w}_b^{t+1} - \delta \boldsymbol{w}_b^{t+1} \tag{37a}$$
$$\boldsymbol{a}_{b'}^{t+1} = \boldsymbol{a}_b^{t+1} - \delta \boldsymbol{a}_b^{t+1} \tag{37b}$$

The transformation matrix $\boldsymbol{M}_{NED}^{t+1|t}$ at time $t+1$ that transforms the data in the IMU body frame into the navigation frame or the NED frame is computed as:

$$\boldsymbol{M}_{NED}^{t+1|t} = \boldsymbol{M}_{NED}^{t|t} \cdot \frac{2\boldsymbol{I}_{3\times3} + \delta\boldsymbol{\Omega}_t \cdot \Delta t}{2\boldsymbol{I}_{3\times3} - \delta\boldsymbol{\Omega}_t \cdot \Delta t}, \tag{38}$$

where, $\delta\boldsymbol{\Omega}_t$ is skew symmetric matrix for angular rate:

$$\delta\boldsymbol{\Omega}_t = \begin{bmatrix} \boldsymbol{0} & -\boldsymbol{w}_{b'}^t(2) & \boldsymbol{w}_{b'}^t(1) \\ \boldsymbol{w}_{b'}^t(2) & \boldsymbol{0} & -\boldsymbol{w}_{b'}^t(0) \\ -\boldsymbol{w}_{b'}^t(1) & \boldsymbol{w}_{b'}^t(0) & \boldsymbol{0} \end{bmatrix} \tag{39}$$

$\boldsymbol{w}_{b'}^t$ is computed by Equ. (37a), and $\boldsymbol{M}_{NED}^{t|t}$ is the last rotation matrix updated by the EKF at the previous step t. At the first time $t+1$ = 1, we can estimate the $\boldsymbol{M}_{NED}^{1|0}$ as

$$\boldsymbol{M}_{NED}^{1|0} = \begin{bmatrix} \boldsymbol{M}_{00} & \boldsymbol{M}_{01} & \boldsymbol{M}_{02} \\ \boldsymbol{M}_{10} & \boldsymbol{M}_{11} & \boldsymbol{M}_{12} \\ \boldsymbol{M}_{20} & \boldsymbol{M}_{21} & \boldsymbol{M}_{22} \end{bmatrix} \tag{40}$$

where, $\boldsymbol{M}_{00} = c(\gamma)c(\beta), \boldsymbol{M}_{01} = c(\gamma)s(\alpha)s(\beta) - c(\alpha)s(\gamma)$, $\boldsymbol{M}_{02} = s(\alpha)s(\gamma) + c(\alpha)c(\gamma)s(\beta), \boldsymbol{M}_{10} = c(\beta)s(\gamma)$, $\boldsymbol{M}_{11} = c(\alpha)c(\gamma) + s(\alpha)s(\gamma)s(\beta), \boldsymbol{M}_{12} = c(\alpha)s(\gamma)s(\beta) - c(\gamma)s(\alpha), \boldsymbol{M}_{20} = -s(\beta), \boldsymbol{M}_{21} = c(\beta)s(\alpha)$, and $\boldsymbol{M}_{22} = c(\alpha)c(\beta)$. Here c and s are $cosine()$ and $sine()$ functions, respectively, and α, β and γ are obtained in Equ. (2).

The EKF error state at time $t+1$ can be obtained by

$$\delta \boldsymbol{X}^{t+1|t+1} = \delta \boldsymbol{X}^{t+1|t} + \boldsymbol{K}^{t+1} \cdot [\boldsymbol{m}^{t+1} - \boldsymbol{H}\delta \boldsymbol{X}^{t+1|t}] \tag{41}$$

where, $\boldsymbol{K}_t$ is the Kalman gain defined in Equ. (44); $\boldsymbol{m}^{t+1}$ is defined in Equ. (31) and $\boldsymbol{H}$ is a measurement matrix:

$$\boldsymbol{H}_{7\times15} = \begin{bmatrix} \boldsymbol{O}_{1\times3}^1 & \boldsymbol{O}_{1\times3}^0 & \boldsymbol{O}_{1\times3}^0 & \boldsymbol{O}_{1\times3}^0 & \boldsymbol{O}_{1\times3}^0 \\ \boldsymbol{O}_{3\times3} & \boldsymbol{I}_{3\times3} & \boldsymbol{O}_{3\times3} & \boldsymbol{O}_{3\times3} & \boldsymbol{O}_{3\times3} \\ \boldsymbol{O}_{3\times3} & \boldsymbol{O}_{3\times3} & \boldsymbol{O}_{3\times3} & \boldsymbol{I}_{3\times3} & \boldsymbol{O}_{3\times3} \end{bmatrix} \tag{42}$$

where, $\boldsymbol{O}^1_{1\times 3}$ = [0 0 1], $\boldsymbol{O}^0_{1\times 3}$ = [0 0 0], $\boldsymbol{I}3\times 3$ is a 3×3 unit matrix, and $\boldsymbol{O}_{3\times 3}$ is a 3×3 zero matrix.
The measurement model of the EKF is defined as

$$\boldsymbol{z}^{t+1} = \boldsymbol{H}\delta\boldsymbol{X}^{t+1|t+1} + \boldsymbol{n}^{t+1} \tag{43}$$

where, $\boldsymbol{n}^{t+1}$ is the measurement noise with covariance matrix $\boldsymbol{R}^{t+1} = \boldsymbol{E}(\boldsymbol{n}^{t+1}(\boldsymbol{n}^{t+1})^T)$.

The Kalman gain is obtained by

$$\boldsymbol{K}^{t+1} = \boldsymbol{P}^{t+1|t}\boldsymbol{H}^T(\boldsymbol{H}\boldsymbol{P}^{t+1|t}\boldsymbol{H}^T + \boldsymbol{R}^{t+1})^{-1}, \tag{44}$$

where $\boldsymbol{P}^{t+1|t}$ is the estimation error covariance matrix which is computed at times $t+1$ of IMU output consequence:

$$\boldsymbol{P}^{t+1|t} = \Phi^t\boldsymbol{P}^{t|t}(\Phi^t)^T + \boldsymbol{Q}^t \tag{45}$$

where, the previous $\boldsymbol{P}^{t|t}$ is computed by the Kalman gain at time t as:

$$\boldsymbol{P}^{t|t} = (\boldsymbol{I}_{15\times 15} - \boldsymbol{K}^t\boldsymbol{H})\boldsymbol{P}^{t|t-1}(\boldsymbol{I}_{15\times 15} - \boldsymbol{K}^t\boldsymbol{H})^T + \boldsymbol{K}^t\boldsymbol{R}^t(\boldsymbol{K}^t)^T \tag{46}$$

Now we can compute the acceleration $\boldsymbol{a}_e^{t+1}$ of human motion in the NED frame by converting the bias-compensated acceleration from Equ. (37b) to the Earth navigation frame NED then subtracting the gravity acceleration vector $\boldsymbol{g}_e$ is in Equ. (6):

$$\boldsymbol{a}_e^{t+1} = \boldsymbol{M}_{NED}^{t+1|t}\cdot\boldsymbol{a}_{b'}^{t+1} - \boldsymbol{g}_e. \tag{47}$$

Then the velocity in the Earth NED frame prior the EKF correction at time $t+1$ is obtained by integrating the acceleration between two consequence outputs of IMU:

$$\boldsymbol{v}^{t+1|t} = \boldsymbol{v}^{t|t} + \boldsymbol{a}_e^{t+1}\cdot\Delta t. \tag{48}$$

This velocity is integrated one more time to compute the foot position in the Earth navigation frame:

$$\boldsymbol{p}^{t+1|t} = \boldsymbol{p}^{t|t} + \boldsymbol{v}^{t+1|t}\cdot\Delta t \tag{49}$$

Finally, we apply the error state vector from EKF in Equ. (41) to correct the values of velocity in Equ. (48), position in Equ. (49), and attitude in Equ. (38).

$$\boldsymbol{v}^{t+1|t+1} = \boldsymbol{v}^{t+1|t} - \delta\boldsymbol{v}^{t+1|t+1} \tag{50}$$

$$\boldsymbol{p}^{t+1|t+1} = \boldsymbol{p}^{t+1|t} - \delta\boldsymbol{p}^{t+1|t+1} \tag{51}$$

$$\boldsymbol{M}_{NED}^{t+1|t+1} = \frac{2\boldsymbol{I}_{3\times 3} + \delta\boldsymbol{\Theta}_t}{2\boldsymbol{I}_{3\times 3} - \delta\boldsymbol{\Theta}_t}\cdot\boldsymbol{M}_{NED}^{t+1|t} \tag{52}$$

where:

$$\delta\boldsymbol{\Theta}^t = -\begin{bmatrix} 0 & -\delta\boldsymbol{\varphi}^t(2) & \delta\boldsymbol{\varphi}^t(1) \\ \delta\boldsymbol{\varphi}^t(2) & 0 & -\delta\boldsymbol{\varphi}^t(0) \\ -\delta\boldsymbol{\varphi}^t(1) & \delta\boldsymbol{\varphi}^t(0) & 0 \end{bmatrix} \tag{53}$$

where, $\delta\boldsymbol{\varphi}^t$ is the EKF error state for attitude at previous time t obtained by Equ. (41).

The summary of the real-time dynamic speed of human foot motion localization algorithm, INS/EKF+ZVU+HDR, is presented in Algorithm 2.

Algorithm 2: REAL-TIME DYNAMIC SPEED OF HUMAN FOOT MOTION LOCALIZATION ALGORITHM (INS/EKF+ZVU+HDR)

$\boldsymbol{Initiate}$ **:** at time $t+1=1$
$\boldsymbol{v}^{1|0} \leftarrow \boldsymbol{0}$
$\boldsymbol{p}^{1|0} \leftarrow \boldsymbol{0}$
$\boldsymbol{M}_{NED}^{1|1} \leftarrow \boldsymbol{M}_{NED}^{1|0}$
$ContinuedLocalization \leftarrow True$
Input: Real-time acceleration, angular rate vectors at time $t+1$ in IMU body system $\langle a_b^{t+1}, w_b^{t+1}\rangle$
Output: Publish the Real-time velocity, position and attitude in NED system: $v^{t+1}, p^{t+1}, M_{NED}^{t+1}$
while $ContinuedLocalization = True$ **do**
  $\delta\boldsymbol{X}^{t|t} \leftarrow \delta\boldsymbol{X}^t(\delta\boldsymbol{\varphi}^t, \delta\boldsymbol{w}^t, \delta\boldsymbol{p}^t, \delta\boldsymbol{v}^t, \delta\boldsymbol{a}_b^t)$
  //DGP is DynamicStanceDetection() function as presented in Algorithm 1.
  if $DGP(a_b^{t+1}, w_b^{t+1}) = True$ **then**
    $\delta\boldsymbol{v}_b^{t+1|t} \leftarrow \boldsymbol{v}_b^{t+1}$
    $\delta\boldsymbol{w}_b^{t+1|t} \leftarrow \boldsymbol{w}_b^{t+1}$
    $\delta\psi^{t+1} \leftarrow HDR(\delta\psi_{\gamma^{T_i}})$
    $\boldsymbol{m}^{t+1} \leftarrow (\delta\psi^{t+1}, \delta\boldsymbol{w}_b^{t+1|t}, \delta\boldsymbol{v}^{t+1|t})$
  else
    $\boldsymbol{m}^{t+1} \leftarrow \boldsymbol{m}^t$
  $\delta\boldsymbol{X}^{t+1|t} \leftarrow \boldsymbol{\Phi}^{t+1}\delta\boldsymbol{X}^{t|t} + \boldsymbol{w}_t$
  $\boldsymbol{P}^{t|t} \leftarrow (\boldsymbol{I}_{15\times 15} - \boldsymbol{K}^t\boldsymbol{H})\boldsymbol{P}^{t|t-1}(\boldsymbol{I}_{15\times 15} - \boldsymbol{K}^t\boldsymbol{H})^T + \boldsymbol{K}^t\boldsymbol{R}^t(\boldsymbol{K}^t)^T$
  $\boldsymbol{P}^{t+1|t} \leftarrow \Phi^t\boldsymbol{P}^{t|t}(\Phi^t)^T + \boldsymbol{Q}^t$
  $\boldsymbol{K}^{t+1} \leftarrow \boldsymbol{P}^{t+1|t}\boldsymbol{H}^T(\boldsymbol{H}\boldsymbol{P}^{t+1|t}\boldsymbol{H}^T + \boldsymbol{R}^{t+1})^{-1}$
  $\delta\boldsymbol{X}^{t+1|t+1} \leftarrow \delta\boldsymbol{X}^{t+1|t} + \boldsymbol{K}^{t+1}\cdot[\boldsymbol{m}^{t+1} - \boldsymbol{H}\delta\boldsymbol{X}^{t+1|t}]$
  $\delta\boldsymbol{w}_b^{t+1|t+1} \leftarrow \delta\boldsymbol{X}^{t+1|t+1}(4:6)$
  $\delta\boldsymbol{a}_b^{t+1|t+1} \leftarrow \delta\boldsymbol{X}^{t+1|t+1}(13:15)$
  $\delta\boldsymbol{v}_b^{t+1|t+1} \leftarrow \delta\boldsymbol{X}^{t+1|t+1}(10:12)$
  $\delta\boldsymbol{p}_b^{t+1|t+1} \leftarrow \delta\boldsymbol{X}^{t+1|t+1}(7:9)$
  $\boldsymbol{w}_{b'}^{t+1} \leftarrow \boldsymbol{w}_b^{t+1} - \delta\boldsymbol{w}_b^{t+1|t+1}$
  $\boldsymbol{a}_{b'}^{t+1} \leftarrow \boldsymbol{a}_b^{t+1} - \delta\boldsymbol{a}_b^{t+1|t+1}$
  $\boldsymbol{M}_{NED}^{t+1|t} \leftarrow \boldsymbol{M}_{NED}^{t|t}\cdot\frac{2\boldsymbol{I}_{3\times 3}+\delta\boldsymbol{\Omega}_t\cdot\Delta t}{2\boldsymbol{I}_{3\times 3}-\delta\boldsymbol{\Omega}_t\cdot\Delta t}$
  $\boldsymbol{a}_e^{t+1} \leftarrow \boldsymbol{M}_{NED}^{t+1|t}\cdot\boldsymbol{a}_{b'}^{t+1} - \boldsymbol{g}_e$
  $\boldsymbol{v}^{t+1|t} \leftarrow \boldsymbol{v}^{t|t} + \boldsymbol{a}_e^{t+1}\cdot\Delta t$
  $\boldsymbol{p}^{t+1|t} \leftarrow \boldsymbol{p}^{t|t} + \boldsymbol{v}^{t+1|t}\cdot\Delta t$
  $\boldsymbol{v}^{t+1|t+1} \leftarrow \boldsymbol{v}^{t+1|t} - \delta\boldsymbol{v}^{t+1|t+1}$
  $\boldsymbol{p}^{t+1|t+1} \leftarrow \boldsymbol{p}^{t+1|t} - \delta\boldsymbol{p}^{t+1|t+1}$
  $\boldsymbol{M}_{NED}^{t+1|t+1} \leftarrow \frac{2\boldsymbol{I}_{3\times 3}+\delta\boldsymbol{\Theta}_t}{2\boldsymbol{I}_{3\times 3}-\delta\boldsymbol{\Theta}_t}\cdot\boldsymbol{M}_{NED}^{t+1|t}$
  if $QuitLocalization = True$ **then**
    $ContinuedLocalization \leftarrow false$
    $Publish(\boldsymbol{v}^{t+1|t+1}, \boldsymbol{p}^{t+1|t+1}, \boldsymbol{M}_{NED}^{t+1|t+1})$
  else
    $Publish(\boldsymbol{v}^{t+1|t+1}, \boldsymbol{p}^{t+1|t+1}, \boldsymbol{M}_{NED}^{t+1|t+1})$
return *True*

V. Verifying Our proposed Algorithm by Ground Truth System

In this section, we validate our proposed INS/EKF ZVU HDR algorithm by using the Motion Tracking System (MTS) from Motion Analysis Corporation [45]. Because the MTS has very high accuracy with only sub-millimeter errors, we can consider this system's tracking results as a Ground Truth. The difference between this system's result and our algorithm's result can be estimated as our algorithm's errors.

We setup the verified experiment relied on MTS as in Fig. 5. The configuration of this MTS included 16 passive optical cameras, in Fig. 5 (2). These cameras are mounted on the pipe system around on the wall of lab. To warrant the MTS can track our shoe as a rigid body, we attached seven markers on it as in Fig. 5 (3).

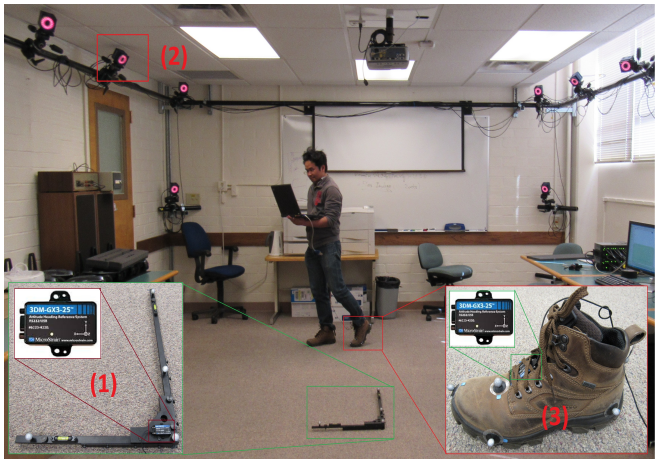

Fig. 5. Using MTS to verify for our proposed algorithm

The tracking operation of the MTS for movement of seven markers attached on the shoe as a rigid body movement shoe is demonstrated by the Fig. 6.

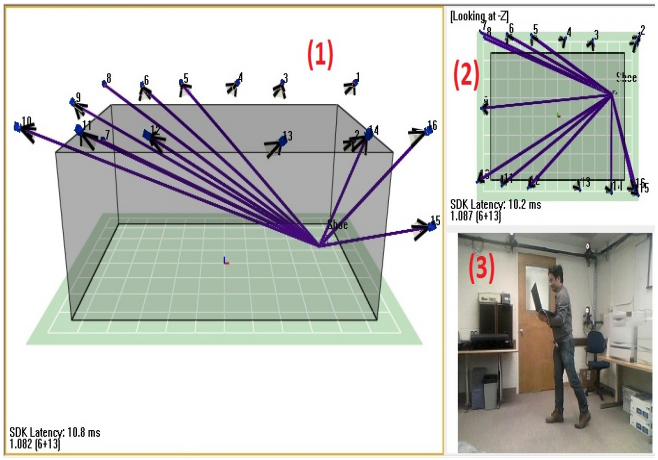

Fig. 6. MTS is tracking the shoe movement around the lab

A. Calibrating MTS and our proposed algorithm.

Because MTS and our proposed algorithm collect and present data in different coordinated systems, a question of validation our proposed algorithm by MTS is how to calibrate them together? We have done this by transforming them into NED system. To transform MTS into NED system, we mounted a 3DM-GX3-25 IMU on a L calibration frame, a tool for calibrating and building coordinate system of the MTS. This L frame is set at the original point of the MTS coordinate system, as in Fig. 5 (1). The X, Y, Z axis of this IMU was mounted equivalently to these axis of MTS system. The Euler angles $Roll$ (α), $Pitch$ (β) and Yaw (γ) of IMU are also the Euler angles of MTS coordinate system. The rotation matrix, $\boldsymbol{R}_M^{t+1}$, to convert MTS data from MTS body system into MTS NED system is obtained by the same formula as $\boldsymbol{M}_{NED}^{1|0}$ in Equ. 40.

$$\boldsymbol{R}_M^{t+1} = \boldsymbol{M}_{NED}^{1|0}. \tag{54}$$

We name a position collected from the MTS for a marker m at time $t+1$ on the shoe in MTS body frame is $\boldsymbol{p}_m^{t+1} = (x_m^{t+1}, y_m^{t+1}, z_m^{t+1})$. The transformed position $\boldsymbol{p}_{mNED}^{t+1}$ of this marker in the MTS NED system is obtained:

$$\boldsymbol{p}_{mNED}^{t+1} = \boldsymbol{R}_M^{t+1} \boldsymbol{p}_m^{t+1}. \tag{55}$$

The moving point of IMU, $\boldsymbol{p}^{t+1|t+1}$, in our proposed algorithm at time $t+1$ is obtained by Equ. (51). Because both markers and IMU are mounted on the same shoe, the starting point of the marker m and IMU in our proposed algorithm at the starting time $t+1=0$ are equivalent, $\boldsymbol{p}_{mNED}^{0} = \boldsymbol{p}^{0|0}$. Otherwise, the $\boldsymbol{p}^{0|0}$ is the original point of the IMU NED system. We have to transform the original position of the IMU NED system into the MTS NED system. So the position of IMU of our proposed algorithm transformed into MTS NED system is obtained:

$$\boldsymbol{p}_{mNED.IMU}^{t+1} = \boldsymbol{p}^{t+1|t+1} + \boldsymbol{p}_{mNED}^{0}. \tag{56}$$

After transforming both MTS and IMU algorithm trajectory data by Equ. (55, 56), we plotted them on the same Fig. 7.

In Fig. 7, the blue trajectory and red trajectory are trajectories tracked by MTS and our IMU algorithm, respectively. The difference between the distances of Starting and Ending points in MTS and proposed algorithm is exactly the error of our algorithm. In this validated experiment, the different distance is 45 mm. The traveling distance in this validation around lab is 13.4 m. So the average error on total traveling distance is approximated 0.335% error. To further demonstrate our proposed algorithm, we plotted the trajectory error between MTS and our algorithm in x and y axises as shown in Fig. 8. As can be seen, the maximum error is small, around 280 mm.

B. The experimental proof of the convergence of our proposed algorithm to MTS.

To prove for our proposed algorithm's result is convergent to MTS's tracking result, we applied the probability density

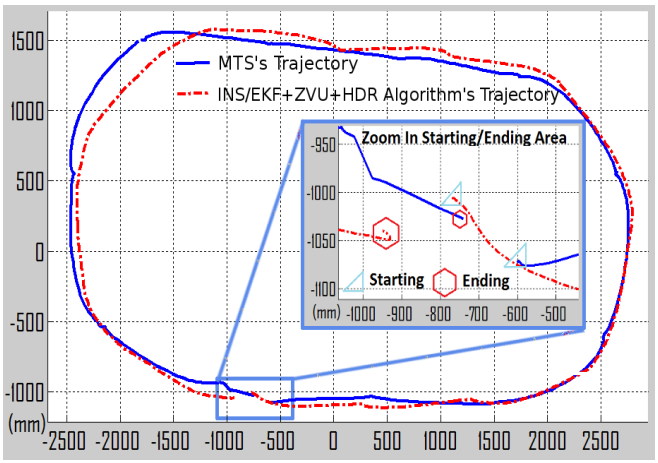

Fig. 7. Plotting trajectories of both MTS and our proposed algorithm

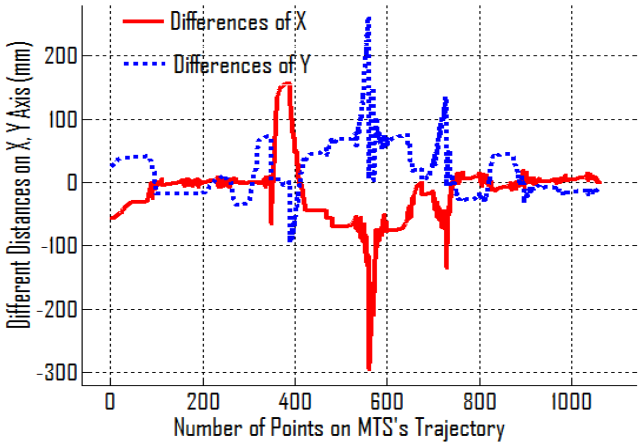

Fig. 8. Error between MTS and our proposed algorithm trajectories in x and y axises.

of difference between them. The different function between them is:

$$\boldsymbol{diff}(\boldsymbol{p}^{t+1}_{mNED}, \boldsymbol{p}^{t+1}_{mNED.IMU}) = (\boldsymbol{p}^{t+1}_{mNED} - \boldsymbol{p}^{t+1}_{mNED.IMU}) \tag{57}$$

The probability density of differences can be computed:

$$\boldsymbol{prob}_{MTS.IMU} = \frac{\boldsymbol{f}(\boldsymbol{diff}(\boldsymbol{p}^{t+1}_{mNED}, \boldsymbol{p}^{t+1}_{mNED.IMU}))}{n} \tag{58}$$

where, $\boldsymbol{f}$ is a frequency function and n is the number of points on MTS's trajectory, $\{\boldsymbol{p}^{t+1}_{mNED}\}$, and $t+1 \in 1...n$. Because the responding rate of MTS and IMU are different. We applied MTS as the GroundTruth for verifying our IMU algorithm. So the total elements n in Equ. (58) is total elements of the data set $\{\boldsymbol{p}^{t+1}_{mNED}\}$. The plotted result of probability density is showed in Fig. 9. The result in this figure has proved that our proposed algorithm's result is convergent to MTS's result. Namely there are about 93.7% localization results of our proposed algorithm which have small error ranges of around 7.5 cm.

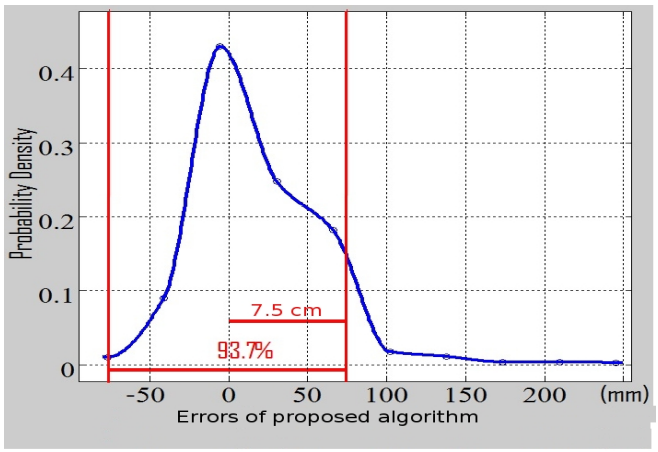

Fig. 9. The convergence of proposed algorithm is over 93% for error range 7.5 cm around MTS's result

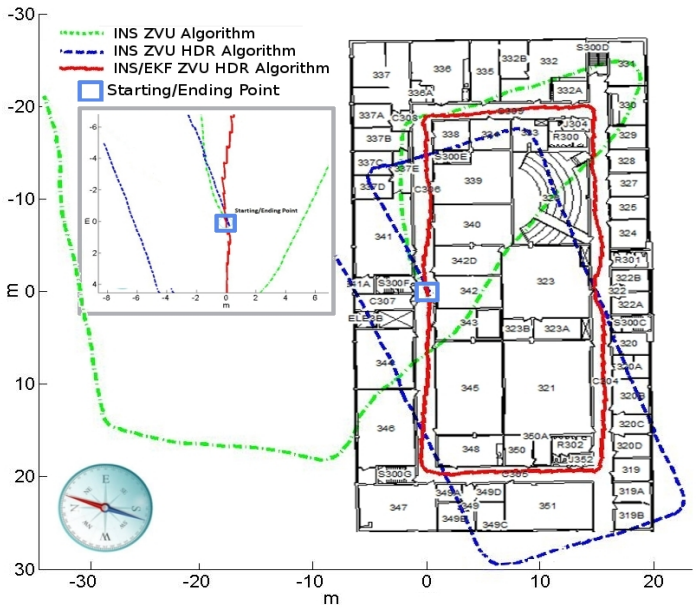

Fig. 10. 2D trajectories plotted in hallway on the 3rd floor plan in SEM building.

VI. Experimental Results

In this section, we implement our proposed algorithm (INS/EKF+ZVU+HDR) and compare it with other algorithms: INS/ZVU and INS/ZVU+HDR. We mount a MicroStrain 3DM-GX3-25 IMU sensor on the shoe for testing the algorithms (see Fig. 5 (3)). We implemented the algorithms by C++ language and ran them on the Hydro ROS (Robotic Operating System) platform. Real-time stream data from 3DM-GX3-25 IMU sensor is processed.

A. Indoor Localization Tests

We tested the algorithms with different walking speeds in the hallway on the 3rd floor of the Scrugham Engineering and

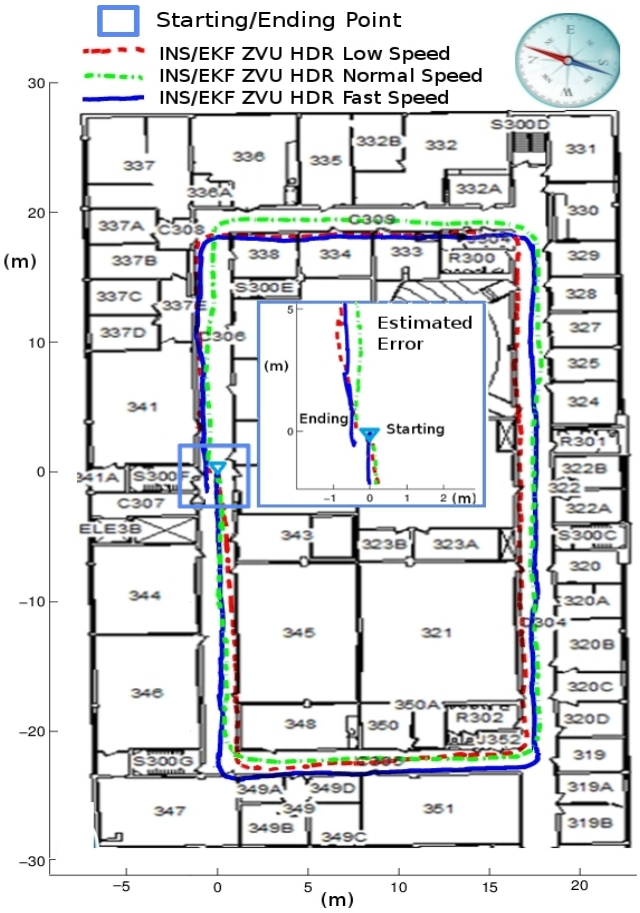

Fig. 11. 2D trajectories of different speeds.

Mines (SEM) building, University of Nevada, Reno (UNR) campus.

Fig. 10 shows the comparison results of three algorithms: INS/ZVU, INS/ZVU+HDR and INS/EKF+ZVU+HDR. We can see that the INS/EKF+ZVU+HDR algorithm outperforms the other twos since its walking trajectory closely matches with the hallway of the SEM building. The average of the different distance between the starting point and ending point in the 2D coordinate for Real-time Dynamic INS/EKF ZVU HDR algorithm is about $0.45m$ over $120m$, equivalent to 0.375% error.

To further demonstrate the effectiveness of the proposed INS/EKF+ZVU+HDR algorithm, we tested it with the different walking speeds which are slow (0.58 m/s), normal (1.28 m/s), and fast (1.79 m/s), respectively. Its results are plotted in Fig. 11. The normal speed trajectory is the green trajectory shows slightly better fit than the other speed trajectories in the hallway. The errors for normal and fast walkings are still good from $0.45m$ and $0.51m$ over $120m$, equivalent around to 0.375% error.

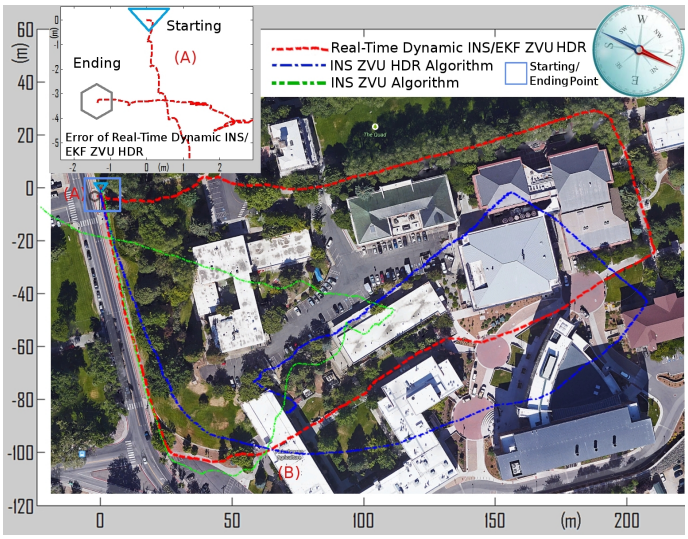

Fig. 12. 2D trajectories of outdoor testing along the sidewalks on UNR campus.

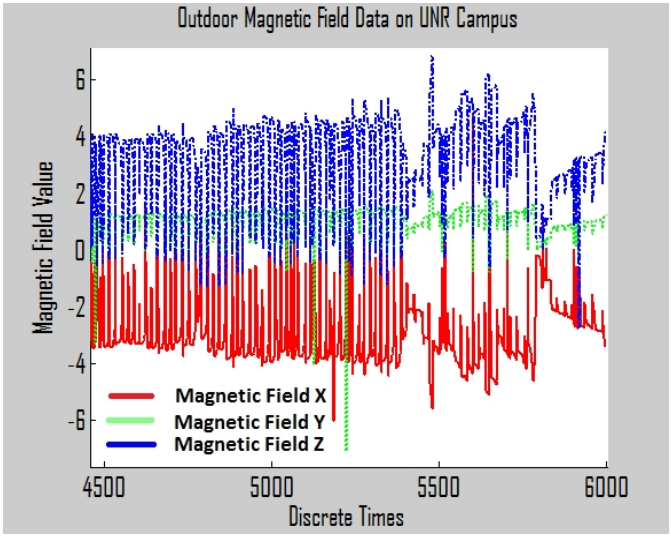

Fig. 13. Outdoor magnetic field data around point (B) in Fig. 12

B. Outdoor Localization Tests

For outdoor environment, we tested and compared our algorithm with the other twos as mentioned above, in a larger scale trajectory along the sidewalks on UNR campus. The results of this test are plotted in Fig. 12. The average of the different distance between the starting point and ending point in the 2D coordinate for this outdoor testing of Real-time Dynamic INS/EKF+ZVU+HDR is about $3.59m$ over $645m$, equivalent to 0.55% error. The zoom-in area (A) in Fig. 12 is a starting/ending point of testing path on UNR campus. The red point (B) in Fig. 12 is the area which shows walking through building gate of an UNR building. There was a large noise of local magnetic disturbances around point (B) as displayed in Fig. 13 due to large steel frames constructed there. This caused the trajectories of the

INS/ZVU and INS/ZVU+HDR algorithms totally turned in wrong directions, but the trajectory of INS/EKF+ZVU+HDR algorithm still shows a very good result.

VII. Conclusion

In this paper, we have proposed a real-time human foot motion localization algorithm using a single IMU device. The proposed algorithm can accurately estimate the human foot position, velocity and attitude with small errors in both indoor and outdoor environments. The proposed algorithm can work with different speeds of human motion like walking, random walk or running. The integration of dynamic human Gait Phase Detection (GPD) with Zero Velocity Update (ZVU) and Extended Kalman Filter (EKF) has significantly removed the IMU drift problems as well as noise in both indoor and outdoor environments. We applied the MTS to verify for our algorithm's results. Real-time localization results of human foot motion have been conducted to show the effectiveness of the proposed algorithm in both indoor and outdoor environments where the disturbances like local magnetic exists.

References

[1] C. Randell, C. Djiallis, and H. Muller, "Personal position measurement using dead reckoning," *Proc. 7th IEEE Int l Symp. Wearable Computers, (ISWC), IEEE CS Press*, pp. 166–173, 2003.

[2] I. Skog, P. Handel, J. Nilsson, and J. Rantakokko, "Zero-velocity detectionan algorithm evaluation," *Biomedical Engineering, IEEE Transactions*, vol. 57, no. 11, pp. 2657–2666, Nov. 2010.

[3] A.R.Jimenez, F. Seco, J. Prieto, and J.Guevara, "Indoor pedestrian navigation using an ins/ekf framework for yaw drift reduction and a foot-mounted imu," *IEEE Positioning Navigation and Communication (WPNC), 7th Workshop*, 2010.

[4] X. Yun, J. Calusdian, E. R. Bachmann, and R. B. McGhee, "Estimation of human foot motion during normal walking using inertial and magnetic sensor measurements," *Instrumentation and Measurement, IEEE Transactions*, vol. 61, no. 7, pp. 2059–2072, Jul. 2012.

[5] E. Foxlin, "Pedestrian tracking with shoe-mounted inertial sensors," *IEEE Computer graphics and Applications*, vol. 1, pp. 38–46, 2005.

[6] Q. Yuan, I. M. Chen, and S. P. Lee, "Slac: 3d localization of human based on kinetic human movement capture," in *Robotics and Automation (ICRA), 2011 IEEE International Conference on*, May 2011, pp. 848–853.

[7] F. Hoflinger, R. Zhang, and L. M. Reindl, "Indoor-localization system using a micro-inertial measurement unit (imu)," in *European Frequency and Time Forum (EFTF)*, April 2012, pp. 443–447.

[8] H. Fourati, N. Manamanni, L. Afilal, and Y. Handrich, "Position estimation approach by complementary filter-aided imu for indoor environment," in *European Control Conference (ECC)*, July 2013, pp. 4208–4213.

[9] N. Corso and A. Zakhor, "Indoor localization algorithms for an ambulatory human operated 3d mobile mapping system," *Remote Sensing*, vol. 5, no. 12, pp. 6611–6646, 2013.

[10] Z. J. Chong, B. Qin, T. Bandyopadhyay, M. H. A. Jr., E. Frazzoli, and D. Rus, "Synthetic 2d lidar for precise vehicle localization in 3d urban environment," *IEEE International Conference on Robotics and Automation (ICRA)*, pp. 1554–1559, May 2013.

[11] J. Schmid, M. Volker, T. Gadeke, P. Weber, W. Stork, and K. Muller-Glaser, "An approach to infrastructure-independent person localization with an ieee 802.15.4 wsn," *2010 INTERNATIONAL CONFERENCE ON INDOOR POSITIONING AND INDOOR NAVIGATION (IPIN)*, Sep. 2010.

[12] J. Saarinen, J. Suomela, S. Heikkila, M. Elomaa, and A. Halme, "Personal navigation system," *IEEERSJ International Conference on Intelligent Robots and Systems IROS*, pp. 212–217, 2004.

[13] J. Corrales, F. Candelas, and F. Torres, "Hybrid tracking of human operators using imu/uwb data fusion by a kalman filter," *ACM/IEEE Int. Conf. Human Robot Interact*, pp. 193–200, 2008.

[14] L. Klingbeil and T. Wark, "A wireless sensor network for real-time indoor localisation and motion monitoring," *Proceedings of the 7th international conference on Information processing in sensor networks. IEEE Computer Society*, p. 3950, May 2008.

[15] A. Ruiz, F. Granja, J. Honorato, and J. Rosas, "Accurate pedestrian indoor navigation by tightly coupling foot-mounted imu and rfid measurements," *IEEE Transactions on Instrumentation and Measurement*, vol. 61, no. 1, Jan. 2012.

[16] S. Soo and S. Park, "Pedestrian inertial navigation with gait phase detection assisted zero velocity updating," *IEEE. In Autonomous Robots and Agents. ICARA 2009 4th International Conference on*, pp. 336–341, May 2009.

[17] H. Liu, H. Darabi, P. Banerjee, and J. Liu, "Survey of wireless indoor positioning techniques and systems," *IEEE Trans. Syst. Man Cybern*, vol. 37, no. 6, pp. 1067–1080, Nov. 2007.

[18] C. Randell, C. Djiallis, and H. Muller, "Personal position measurement using dead reckoning," *Seventh IEEE International Symposium on Wearable Computers 2003 Proceedings*, pp. 166–173, 2003.

[19] Q. Ladetto, "On foot navigation : continuous step calibration using both complementary recursive prediction and adaptive kalman filtering," *ION GPS*, vol. 2000, pp. 1735–1740, 2000.

[20] J. W. Kim and C. Park, "A step , stride and heading determination for the pedestrian navigation system," *Technology*, vol. 3, no. 1, pp. 273–279, 2005.

[21] R. Stirling, J. Collin, K. Fyfe, and G. Lachapelle, "An innovative shoe-mounted pedestrian navigation system," *GNSS*, 2003.

[22] S. Godha, G. Lachapelle, and M. E. Cannon, "Integrated gps/ins system for pedestrian navigation in a signal degraded environment," *ION GNSS*, vol. 2006, pp. 26–29, 2006.

[23] A. R. Jimenez, F. Seco, C. Prieto, and J. Guevara, "A comparison of pedestrian dead-reckoning algorithms using a low-cost mems imu," *2009 IEEE International Symposium on Intelligent Signal Processing*, pp. 37–42, 2009.

[24] N. Castaneda and S. Lamy-Perbal, "An improved shoe-mounted inertial navigation system," *International Conference on Indoor Positioning and Indoor Navigation - IEEE*, pp. 1–6, Sep. 2010.

[25] F. Cavallo, A. Sabatini, and V. Genovese, "A step toward gps/ins personal navigation systems: real-time assessment of gait by foot inertial sensing," *IEEE/RSJ International Conference on Intelligent Robots and Systems*, pp. 1187–1191, 2005.

[26] S. Park, "Pedestrian inertial navigation with gait phase detection assisted zero velocity updating," *2009 4th International Conference on Autonomous Robots and Agents. IEEE*, pp. 336–341, Feb. 2000.

[27] S. Yang and Q. Li, "Ambulatory walking speed estimation under different step lengths and frequencies," *2010 IEEE/ASME International Conference on Advanced Intelligent Mechatronics*, vol. 24, no. 17, pp. 658–663, Jul. 2010.

[28] C. Toth, D. A. Grejner-Brzezinska, and S. Moafipoor, "Pedestrian tracking and navigation using neural networks and fuzzy logic," *2007 IEEE International Symposium on Intelligent Signal Processing. IEEE*, pp. 1–6, 2007.

[29] L. Fang, P. Antsaklis, L. Montestruque, M. McMickell, M. Lemmon, Y. Sun, H. Fang, I. Koutroulis, M. Haenggi, M. Xie, and X. Xie, "Design of a wireless assisted pedestrian dead reckoning systemthe navmote experience," *IEEE Trans. Instrum. Meas.*, vol. 54, no. 6, pp. 2342–2358, Dec. 2005.

[30] P. Goyal, V. J. Ribeiro, H. Saran, and A. Kumar, "Strap-down pedestrian dead-reckoning system," *International Conference on Indoor Positioning and Indoor Navigation-IEEE*, pp. 1–7, Sep. 2011.

[31] L. Ojeda and J. Borenstein, "Non-gps navigation with the personal dead-reckoning system," *Proc. SPIE*, vol. 6561, no. 1, 2007.

[32] U. Steinhoff and B. Schiele, "Dead reckoning from the pocket - an experimental study," *IEEE International Conference*, pp. 162–170, Apr. 2010.

[33] P. Groves, G. Pulford, C. Mather, A. Littlefield, D. Nash, and M. Carter, "Integrated pedestrian navigation using gnss, mems imu, magnetometer and baro-altimeter," *In The Navigation Conference and Exhibition (NAV 2007)*, 2007.

[34] J. Georgy, A. Noureldin, M. Korenberg, and M. Bayoumi, "Modeling the stochastic drift of a mems-based gyroscope in gyro/odometer/gps

integrated navigation," *IEEE Trans. Intell. Transp. Syst*, vol. 11, no. 4, pp. 856–872, Dec. 2010.

[35] L. Chen and H. Hu, "Imu/gps based pedestrian localization," *IEEE. Computer Science and Electronic Engineering Conference (CEEC)*, pp. 23–28, Sep. 2012.

[36] M. G. Puyol, D. Bobkov, P. Robertson, and T. Jost, "Pedestrian simultaneous localization and mapping in multistory buildings using inertial sensors," *IEEE Transaction on Intelligent Transportation Systems*, vol. 15, no. 4, pp. 1714–1727, Aug. 2014.

[37] J. Hesch, F. Mirzaei, G. Mariottini, and S. Roumeliotis, "A laser-aided inertial navigation system (l-ins) for human localization in unknown indoor environments," *Proc. IEEE Int. Conf. Robot*, p. 53765382, 2010.

[38] G. Welch and G. Bishop, "An introduction to the kalman filter," *University of North Carolina at Chapel Hill*, p. 116, 1995.

[39] S. Bolognani, L. Tubiana, and M. Zigliotto, "Extended kalman filter tuning in sensorless pmsm drives," *IEEE Transactions on Industry Applications*, vol. 39, no. 6, pp. 1741–1747, Nov. 2003.

[40] F. Zampella, M. Khider, P. Robertson, and A. Jimenez, "Unscented kalman filter and magnetic angular rate update (maru) for an improved pedestrian dead-reckoning," *Proc. IEEE/ION PLANS*, p. 129139, Apr. 2012.

[41] S. Beauregard and M. Widyawan, "Indoor pdr performance enhancement using minimal map information and particle filters," *Proc. IEEE/ION PLANS*, p. 141147, May 2008.

[42] W. George and I. Collins, *The Foundations of Celestial Mechanics*. US: The Pachart Foundation dba Pachart Publishing House and reprinted by permission, 2004.

[43] H. Zhang, J. Qian, L. Shen, and Y. Zhang, "Research on healthy subject gait cycle phase at different walking speeds," *Robotics and Biomimetics (ROBIO), 2012 IEEE International Conference on*, pp. 1349–1354, Dec. 2012.

[44] J. Borestein, L. Ojeda, and S. Kwanmuang, "Heuristic reduction of gyro drift in imu-based personnel tracking system," *SPIE Defense, Security and Sensing Conference*, pp. 1–11, Apr. 2009.

[45] "Motion analysis corporation," *http://http://www.motionanalysis.com/*, 1999.